

photographic emulsion. This parameter is<sup>15</sup>

$$P = (29.1 \pm 0.7) / (598.5 \pm 1) = 4.86 \pm 0.12 \text{ percent.}$$

<sup>15</sup> If the emulsion thickness  $t$  is less than the range  $r$  of a  $\mu$ -meson, the longer tracks have a higher probability of escaping from the emulsion. The probability of a  $\mu$ -meson which originates in the emulsion also stopping in it is  $t/2r$ . Thus, if the  $\mu$ -meson ranges would be normally distributed in an infinite emulsion, their distribution in a thin emulsion would be  $(K/r) \exp[-(r-\bar{r})^2/2\sigma^2]$ . It can be shown that this distribution can be approximated by a normal distribution with the same standard deviation and a displaced mean,  $K' \exp[-(r-\bar{r}-\Delta)^2/2\sigma^2]$ , with more accuracy than could be detected in this study, by expanding  $K/r$  in a Taylor's series about  $\bar{r}$  and showing that the series expansion of

We are indebted to Dr. R. Sagane for making his photographic plates available to us. Professor J. K. Knipp has provided invaluable stimulation, advice, and discussion in the process of this work. The suggestions and criticism of Professor Oscar Kempthorne of the Iowa State College Department of Statistics have been extremely welcome and useful.

$K' \exp\{2(r-\bar{r})\Delta - \Delta^2\}/2\sigma^2\}$  sufficiently approximates this Taylor's series when  $\Delta = -\sigma^2/\bar{r}$ . Thus, an experimentally obtained range distribution has a mean about 1.5 microns less than the value to be expected in infinite emulsion.

## Total Compton and Pair Production Cross Sections at 19.5 Mev\*

ARTHUR I. BERMAN†

*University of California, Los Alamos Scientific Laboratory, Los Alamos, New Mexico*

(Received January 6, 1953)

Total cross sections of 19 elements were measured at 19.5 Mev by the photonuclear detector method. The penetration of betatron bremsstrahlung (maximum energy, 20.4 Mev) through the absorbers was determined by the  $C^{22}(\gamma, n)C^{21}$  reaction (threshold, 18.7 Mev) in polyethylene. Simultaneously operated monitor-detector Geiger units, which canceled timing and intensity fluctuation errors, recorded the carbon-11 activity. Percent standard deviations averaged 0.6 for most elements; the estimated systematic error was 0.4 percent. The narrow energy band width permitted an accurate calculation of the correction for the proportion of counts due to secondary radiation.

From the absorption data a value of the Compton cross section was determined. The integrated Klein-Nishina result fell within the 2 percent experimental error calculated by adding linearly to the statistical errors, an estimated 50 percent uncertainty in the published photonuclear cross sections employed in the determination. The cross sections for pair production found from the experiment  $\sigma_e$ , are related to the theoretical values  $\sigma_t$ , as derived by the Born approximation (Bethe-Heitler formula including screening), by  $(\sigma_e - \sigma_t)/\sigma_t = (1.55 \pm 0.1) \times 10^{-9} Z^2$ , to a first approximation.

### I. SUMMARY OF THE THEORY OF ABSORPTION OF HIGH ENERGY QUANTA

OF the major processes by which high energy photons interact with matter<sup>1</sup>—Compton effect, pair production, triplet production, atomic photoelectric effect, and photonuclear reactions—the first two account for nearly all of the total absorption cross section in all elements at high relativistic energies.

The differential cross section for the Compton effect was calculated by Klein and Nishina on the assumption that the interacting electrons have zero binding energy.<sup>2</sup> The integration is elementary,<sup>3</sup> and the result has been verified at many low energies.<sup>4</sup>

\* Work performed under the auspices of the U. S. Atomic Energy Commission. A preliminary report was given to the American Physical Society, Berkeley meeting (December 27–29, 1951).

† Present address: Stanford University, Stanford, California.

<sup>1</sup> A more complete discussion of these absorption processes may be found in A. I. Berman, Los Alamos Document, LAMD 1088 (unpublished).

<sup>2</sup> O. Klein and Y. Nishina, *Z. Physik* **52**, 853 (1929).

<sup>3</sup> W. Heitler, *The Quantum Theory of Radiation* (Oxford University Press, London, 1944), second edition, p. 157.

<sup>4</sup> S. J. M. Allen, *Phys. Rev.* **27**, 266 (1926); G. T. B. Tarrant, *Proc. Roy. Soc. (London)* **128**, 345 (1930); G. E. M. Jauncy and

The cross section for the production of pairs in the nuclear field has been derived, with the aid of the Born approximation, by Bethe and Heitler.<sup>5</sup> The treatment included the effect of screening of the nuclear potential by the atomic electrons based on the assumption of a Thomas-Fermi atomic model. The pair cross section was recalculated by Maximon, Davies, and Bethe, using Coulomb wave functions.<sup>6</sup>

Triplet production, or the creation of pairs in the field of an electron, resulting in the ejection of the three particles has been studied by Wheeler and Lamb<sup>7</sup> in a manner similar to the analysis of nuclear pair production by Bethe and Heitler. The cross section per atom is approximately  $1/Z$  that of pair production; this ratio varies little with energy or  $Z$ .

The relativistic theory of high energy photoelectric absorption in the  $K$  shell was developed rigorously by

G. G. Harvey, *Phys. Rev.* **37**, 698 (1931); J. Read and C. C. Lauritsen, *Phys. Rev.* **45**, 433 (1934); L. Meitner and H. Hupfeld, *Z. Physik* **67**, 147 (1940).

<sup>5</sup> H. Bethe and W. Heitler, *Proc. Roy. Soc. (London)* **146**, 83 (1934).

<sup>6</sup> L. C. Maximon and H. A. Bethe, *Phys. Rev.* **87**, 156 (1952); H. Davies and H. A. Bethe, *Phys. Rev.* **87**, 156 (1952).

<sup>7</sup> J. A. Wheeler and W. E. Lamb, *Phys. Rev.* **55**, 858 (1939).

Hall.<sup>8</sup> Following some empirical and theoretical evidence that the photoelectric cross section for the entire atom is 5/4 of the *K*-shell result,<sup>9</sup> a theoretical value of the atomic cross section may be given to fair accuracy at 20 Mev.

Photonuclear reactions make a small, but not negligible, contribution to the total absorption cross section, especially centered in the 20-Mev region. The Goldhaber-Teller high frequency resonance theory has received considerable attention.<sup>10</sup> Alternative theories have been given;<sup>11</sup> for example, Levinger and Bethe explained the absorption of quanta by nuclei in terms of dipole transitions, where sum rules are used to calculate both the integrated cross section (over all quantum energies) and the mean energy for quantum absorption. At several hundred Mev, photonuclear cross sections, possibly due to mesonic effects, again become significant.<sup>12</sup>

In comparison with these five processes, coherent scattering by atomic electrons as well as nuclear scattering cross sections are negligible.

Existing measured absorption data near the beginning of the extreme relativistic region ( $\sim 20$  Mev)<sup>13,14</sup> have permitted neither a calculation of the Compton cross section nor an accurate quantitative expression for the failure of the Born approximation in the theory of pair production in heavy elements.

## II. EXPERIMENTAL TOTAL ABSORPTION CROSS SECTIONS AT 19.5 MEV

### A. Design of the Experiment

The continuous x-ray spectrum of a betatron was used as the source of photons in this experiment. A narrow energy band was isolated by a threshold detector method,<sup>13</sup> in which the maximum energy  $\epsilon_M$  was adjusted to be slightly greater than the threshold energy  $\epsilon_T$  of the detecting reaction  $C^{12}(\gamma, n)C^{11}$ . Since this band is located in a region in which the total absorption cross section is a slowly varying function of energy, only a small uncertainty is introduced when estimating the centroid of the band. The approximate energy distribution of bremsstrahlung,  $I_\epsilon$ , is shown in Fig. 1; it is weighted by the assumed detecting reaction cross section function  $\sigma_\epsilon$  near threshold to produce the lower curve of effective intensity.

The radiation traverses the polyethylene monitor, penetrates the absorber of known mass per unit area  $t$ ,

<sup>8</sup> H. Hall, *Revs. Modern Phys.* **8**, 359 (1936); H. Hall, *Phys. Rev.* **84**, 167 (1951).

<sup>9</sup> Rutherford, Chadwick, and Ellis, *Radiations from Radioactive Substances* (Cambridge University Press, Cambridge, 1930), p. 464; H. Hall and W. Rarita, *Phys. Rev.* **46**, 143 (1934).

<sup>10</sup> W. Goldhaber and E. Teller, *Phys. Rev.* **74**, 1046 (1948).

<sup>11</sup> R. D. Present, *Phys. Rev.* **77**, 355 (1950); J. S. Levinger and H. A. Bethe, *Phys. Rev.* **78**, 115 (1950); Steinwedel, Jensen, and Jensen, *Phys. Rev.* **79**, 1019 (1950); E. D. Courant, *Phys. Rev.* **82**, 703 (1951).

<sup>12</sup> L. Jones, thesis, University of California, UCRL 1916 (August, 1952) (unpublished).

<sup>13</sup> G. D. Adams, *Phys. Rev.* **74**, 1707 (1948).

<sup>14</sup> R. L. Walker, *Phys. Rev.* **76**, 527 (1949); **76**, 1440 (1949).

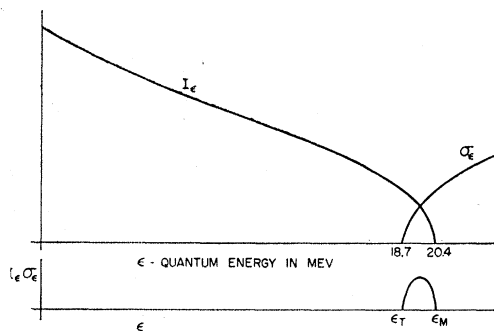


FIG. 1. Energy band used in the absorption experiments. Within the band, parabolic distributions of betatron intensity  $I_\epsilon$  and  $C^{12}(\gamma, n)C^{11}$  cross section  $\sigma_\epsilon$  have been assumed. This is based on experimental evidence that  $\int I_\epsilon \sigma_\epsilon d\epsilon = k_1(\epsilon_M - \epsilon_T)^2$ , and theoretical evidence that  $\sigma_\epsilon = k_2(\epsilon - \epsilon_T)^2$ , near threshold.

and then strikes the polyethylene detector, as shown schematically in Fig. 2. Polyethylene was chosen because of its high purity and low adsorption of atmospheric nitrogen and oxygen. Following the exposure, the monitor and detector cylinders are placed around two simultaneously operated Geiger counters, and the total number of counts, in thirty minutes, of the resulting carbon-11 positron activity is recorded. The procedure is repeated without the absorber, using the same set of cylinders, after the activity has decreased to a negligible value. The mass absorption coefficient at the effective energy of the band is given by

$$\mu = t^{-1} \ln(D_0 M / D M_0), \quad (1)$$

where  $M$ ,  $D$  and  $M_0$ ,  $D_0$  refer to the monitor and detector counts with and without the absorber in place, respectively. Fluctuations in intensity, quantum energy, and exposure and counting times, from run to run, are canceled automatically by using this technique. Rapid counting rates were obtained by performing the experiment within the betatron air gap close to the donut and exposing for nearly the 20.5-minute half-life of the activity. Absorber thicknesses were chosen, by considerations of geometry as well as statistics, to be approximately one mean free path of 19.5-Mev quanta, where convenient. A monitor-absorber-detector assembly constructed of Lucite enabled the relative positions of components to be maintained to within several thousandths of an inch during the weeks of operation.

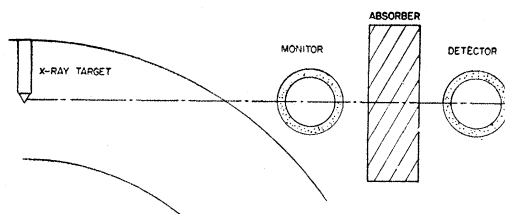


FIG. 2. A schematic view of the experimental arrangement of the absorber and the polyethylene monitor and detector cylinders.

TABLE I. Theoretical cross sections per atom at 19.5 Mev in barns.

| Element | Photoelectric (Hall) | Compton (Klein-Nishina) | Pair (Bethe-Heitler) | Triplet (Wheeler-Lamb) | Photoneuclear (semi-empirical) | Total  |
|---------|----------------------|-------------------------|----------------------|------------------------|--------------------------------|--------|
| H       | ...                  | 0.0308                  | 0.0032               | 0.0032                 | ...                            | 0.0372 |
| C       | ...                  | 0.185                   | 0.115                | 0.018                  | 0.005                          | 0.323  |
| Mg      | ...                  | 0.370                   | 0.455                | 0.038                  | 0.033                          | 0.896  |
| Al      | ...                  | 0.401                   | 0.534                | 0.041                  | 0.043                          | 1.019  |
| Fe      | 0.001                | 0.802                   | 2.114                | 0.082                  | 0.090                          | 3.089  |
| Cu      | 0.001                | 0.894                   | 2.627                | 0.090                  | 0.110                          | 3.722  |
| Zn      | 0.002                | 0.925                   | 2.808                | 0.095                  | 0.100                          | 3.930  |
| Ag      | 0.014                | 1.449                   | 6.846                | 0.145                  | 0.10                           | 8.55   |
| Cd      | 0.016                | 1.480                   | 7.136                | 0.150                  | 0.10                           | 8.88   |
| Sn      | 0.019                | 1.542                   | 7.732                | 0.154                  | 0.10                           | 9.55   |
| Sb      | 0.021                | 1.573                   | 8.045                | 0.156                  | 0.10                           | 9.90   |
| Ta      | 0.10                 | 2.25                    | 16.34                | 0.22                   | 0.15                           | 19.06  |
| W       | 0.11                 | 2.28                    | 16.79                | 0.23                   | 0.15                           | 19.56  |
| Pt      | 0.14                 | 2.41                    | 18.63                | 0.24                   | 0.15                           | 21.57  |
| Au      | 0.15                 | 2.44                    | 19.11                | 0.25                   | 0.15                           | 22.10  |
| Pb      | 0.18                 | 2.53                    | 20.58                | 0.26                   | 0.15                           | 23.65  |
| Bi      | 0.19                 | 2.56                    | 21.07                | 0.27                   | 0.15                           | 24.24  |
| Th      | 0.26                 | 2.78                    | 24.73                | 0.28                   | 0.15                           | 28.20  |
| U       | 0.28                 | 2.84                    | 25.80                | 0.29                   | 0.15                           | 29.36  |

## B. Determination of the Effective Energy

The quantum energy of a monoenergetic beam, which would be absorbed in the material to the same degree as the entire band, is found by considering (1) the centroid of the band and (2) the calibration of the betatron.

### 1. The Centroid

If the total absorption cross section is expanded in powers of the quantum energy above threshold,  $\epsilon - \epsilon_T$ , and nonlinear terms are neglected, then the centroid of the band is calculated to be

$$\epsilon' - \epsilon_T = \frac{\int_{\epsilon_T}^{\epsilon_M} (\epsilon - \epsilon_T) I_e \sigma_e d\epsilon}{\int_{\epsilon_T}^{\epsilon_M} I_e \sigma_e d\epsilon}, \quad (2)$$

where  $\epsilon'$  is the effective energy.

It was found experimentally, by observing the polyethylene counting rate  $Y$  at various operating energies, that

$$Y(\epsilon_M) = k_0 \int_{\epsilon_T}^{\epsilon_M} I_e \sigma_e d\epsilon = k_1 (\epsilon_M - \epsilon_T)^2; \quad \epsilon_M - \epsilon_T \ll \epsilon \quad (3)$$

(where the  $k$ 's are constants), agreeing with other workers. This equation holds for either the incident photon density or the intensity density function because of the restriction on the energy band width. It is known from theory that the detecting reaction photodisintegration cross section  $\sigma_e$  near threshold is proportional to  $(\epsilon - \epsilon_T)^{1/2}$ .<sup>15</sup>

From this fact and Eq. (3) it follows that  $I_e$  is proportional to  $(\epsilon_M - \epsilon)^{1/2}$ . Actually little is known otherwise of the shape of high energy bremsstrahlung near cutoff;

<sup>15</sup> J. M. Blatt and V. F. Weisskopf, *Theoretical Nuclear Physics* (John Wiley and Sons, Inc., New York, 1952), pp. 609, 656.

theoretical calculations<sup>16</sup> are based on the assumption that the electron velocity is on the order of the velocity of light. But this condition is invalid at the high energy end of the spectrum, where the recoil electron has transferred nearly all of its kinetic energy to the quantum. It is true, however, that for *thin* targets, one may state the existence of a finite bremsstrahlung cross section at high energy cutoff by extension of the exact nonrelativistic equation.<sup>5</sup>

Solving Eq. (2), one obtains

$$\epsilon' = \frac{1}{2}(\epsilon_M + \epsilon_T). \quad (4)$$

### 2. Calibration of the Betatron

The threshold energy  $\epsilon_T$  is found from mass measurements<sup>17</sup> as  $18.71 \pm 0.05$  Mev (where account is taken of the recoil of the carbon-12 nucleus).

The operating energy of the betatron,  $\epsilon_M$ , controlled by adjusting the effective value of the magnetic field strength, is found in the following manner: A voltmeter linked with the changing field registers a deflection which is proportional to the maximum field strength and therefore to the momentum of the electrons as they strike the target. (The energy radiated by acceleration of the electrons in the orbit is negligible at 20 Mev.) The calibration equation then follows from the relativistic kinetic energy formula

$$\epsilon_M = [(KD)^2 + (m_0c^2)^2]^{1/2} - m_0c^2, \quad (5)$$

where  $K$  = calibration constant,  $D$  = meter reading,

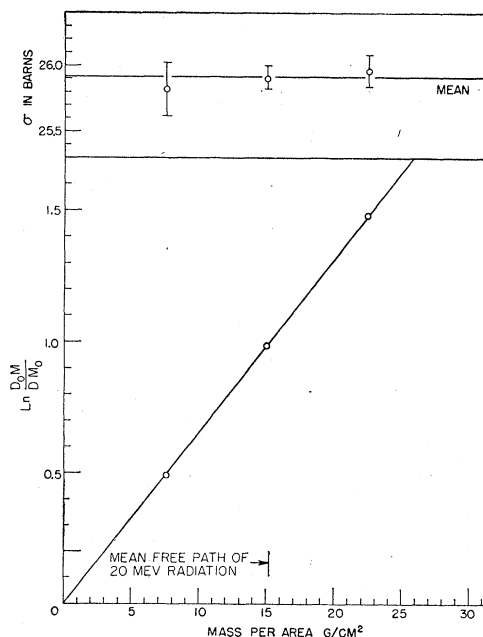


FIG. 3. Exponential absorption in uranium.

<sup>16</sup> L. I. Schiff, *Phys. Rev.* **83**, 252 (1951); see also reference 6.

<sup>17</sup> H. A. Bethe, *Elementary Nuclear Theory* (John Wiley and Sons, Inc., New York, 1947), p. 124; Li, Whaling, Fowler, and Lauritsen, *Phys. Rev.* **83**, 512 (1951).

$m_0$ =electron rest mass, and  $c$ =velocity of light. By operating the betatron at several values of  $D$ , noting the counting rate each time and extrapolating to zero counting rate (at this point,  $\epsilon_M = \epsilon_T$ ), the value of  $K$  is determined. In this manner, the operating energy  $\epsilon_M$  was found, and the effective energy was adjusted to be 19.5 Mev from Eq. (4).

### C. Computed Results

#### 1. Correction for Scattered Radiation

Since part of the scattered radiation has energy  $\epsilon > \epsilon_T$  and will therefore induce the  $C^{12}(\gamma, n)$  reaction of the detector, the absorption coefficient will be misinterpreted as being lower than its true value, necessitating a correction. Effects from high velocity photoelectric, Compton, and pair electrons may be shown to be negligible, despite their relatively large numbers. When operating the betatron slightly below 18.7 Mev, no secondary nuclear emanations were discovered which induced monitor or detector activity, with the exception of photofission products in uranium and thorium. Both elements were bombarded, therefore, in Lucite shields to prevent this contamination.

The number of counts due to primary, or undeflected, quanta  $C_p$  is related to the observed number of counts  $C_0$  and that due to scattered quanta  $C_s$  by

$$C_p = C_0 - C_s = C_0(1 - C_s/C_0) \cong C_0(1 - C_s/C_p). \quad (6)$$

The ratio of secondary to primary counts may be calculated (see Appendix) as

$$C_s/C_p = \frac{1}{3} \pi n_e r_0^2 R_0 \theta_0^2, \quad (7)$$

where  $n_e$ =electron density,  $r_0$ =classical electron radius,  $R_0$ =absorber thickness, and  $\theta_0$ =maximum angle of detected scattered radiation. For the energy band width used in the experiment,  $\theta_0$  is less than 4 degrees; therefore, the correction for singly scattered radiation in all absorbers amounted to a few tenths of one percent. The correction for multiply scattered radiation is consequently completely negligible.

#### 2. Other Corrections

Halogen-filled Geiger tubes of high stability and long lifetimes permitted the use of rapid counting rates ( $\sim 150$  cps). A small systematic error was present when the counting rate was corrected for dead time because of the uncertainty in second-order effects in counter resolution theory. Periodic checks with standard sources insured counting reproducibility. Additional corrections which were made, *viz.*, counter background, shifting of  $\epsilon_M$  due to power line frequency fluctuations, thermal expansion of the absorbers by induction heating, traces of absorber impurities, and the fact that a divergent rather than parallel beam penetrated the absorber, amounted to less than one percent.

The total systematic error in the absorption cross sections, found by adding together conservative esti-

TABLE II. Experimental cross sections per atom at 19.5 Mev.

| Element | $\sigma_{tot}$<br>(barns) | Standard deviation<br>(percent) | $\mu_m$<br>(cm <sup>2</sup> /g) |
|---------|---------------------------|---------------------------------|---------------------------------|
| H       | 0.0377±0.0034             | 9                               | 0.0226                          |
| C       | 0.3142±0.0037             | 1.0                             | 0.01576                         |
| Mg      | 0.909 ±0.011              | 1.2                             | 0.02252                         |
| Al      | 1.006 ±0.003              | 0.3                             | 0.02249                         |
| Fe      | 3.058 ±0.021              | 0.7                             | 0.03300                         |
| Cu      | 3.714 ±0.019              | 0.5                             | 0.03522                         |
| Zn      | 3.905 ±0.015              | 0.4                             | 0.03598                         |
| Ag      | 8.34 ±0.05                | 0.6                             | 0.04659                         |
| Cd      | 8.63 ±0.04                | 0.5                             | 0.04628                         |
| Sn      | 9.23 ±0.05                | 0.5                             | 0.04687                         |
| Sb      | 9.54 ±0.04                | 0.4                             | 0.04720                         |
| Ta      | 17.92 ±0.12               | 0.7                             | 0.05970                         |
| W       | 18.16 ±0.05               | 0.3                             | 0.05949                         |
| Pt      | 19.92 ±0.18               | 0.9                             | 0.06148                         |
| Au      | 20.15 ±0.18               | 0.9                             | 0.01656                         |
| Pb      | 21.58 ±0.06               | 0.3                             | 0.06275                         |
| Bi      | 21.93 ±0.09               | 0.4                             | 0.06322                         |
| Th      | 25.10 ±0.22               | 0.9                             | 0.06516                         |
| U       | 25.91 ±0.07               | 0.3                             | 0.06558                         |

mates (20 to 50 percent) of uncertainties in the above corrections was about 0.2 percent for most absorbers and slightly higher for several of the low  $Z$  absorbers. To this is added the estimated systematic error involved in the assumptions and procedures used in establishing the effective energy by Eq. (4),  $\pm 0.15$  Mev, in terms of the effect on the slowly varying total cross section. This ranged from 0.0 percent for magnesium to 0.25 for uranium. A conservative estimate of the upper limit of the total systematic error would therefore be  $\sim 0.4$  percent for all absorbers, assuming that all possible sources of error have been considered.

#### 3. Verification of Exponential Absorption

In the experiments on uranium, three absorbers were measured of thickness:  $\frac{1}{2}$ , 1, and  $1\frac{1}{2}$  mean free paths of 20-Mev photons. A plot of  $\ln(D_0M/DM_0)$  vs mass per area,  $t$ , is shown in Fig. 3 to yield a straight line. On an expanded scale, the total cross section at the three points is given also (including the standard deviation); the constancy confirms the use of the exponential absorption law in calculating total absorption cross sections.

#### 4. Absorption Cross Sections

Theoretical cross sections are listed in Table I for the absorption processes discussed in Sec. I. The term absorption is used as a synonym for interaction, *i.e.*, to a detector of infinite energy resolution, a quantum loses its original identity in *any* process. The pair cross sections listed are those computed from the formula of Bethe and Heitler, where the effect of screening is calculated as a correction to the unscreened value. The photonuclear cross sections which are given are estimated from the considerable empirical data available on photonucleon yields and radioactive measurements

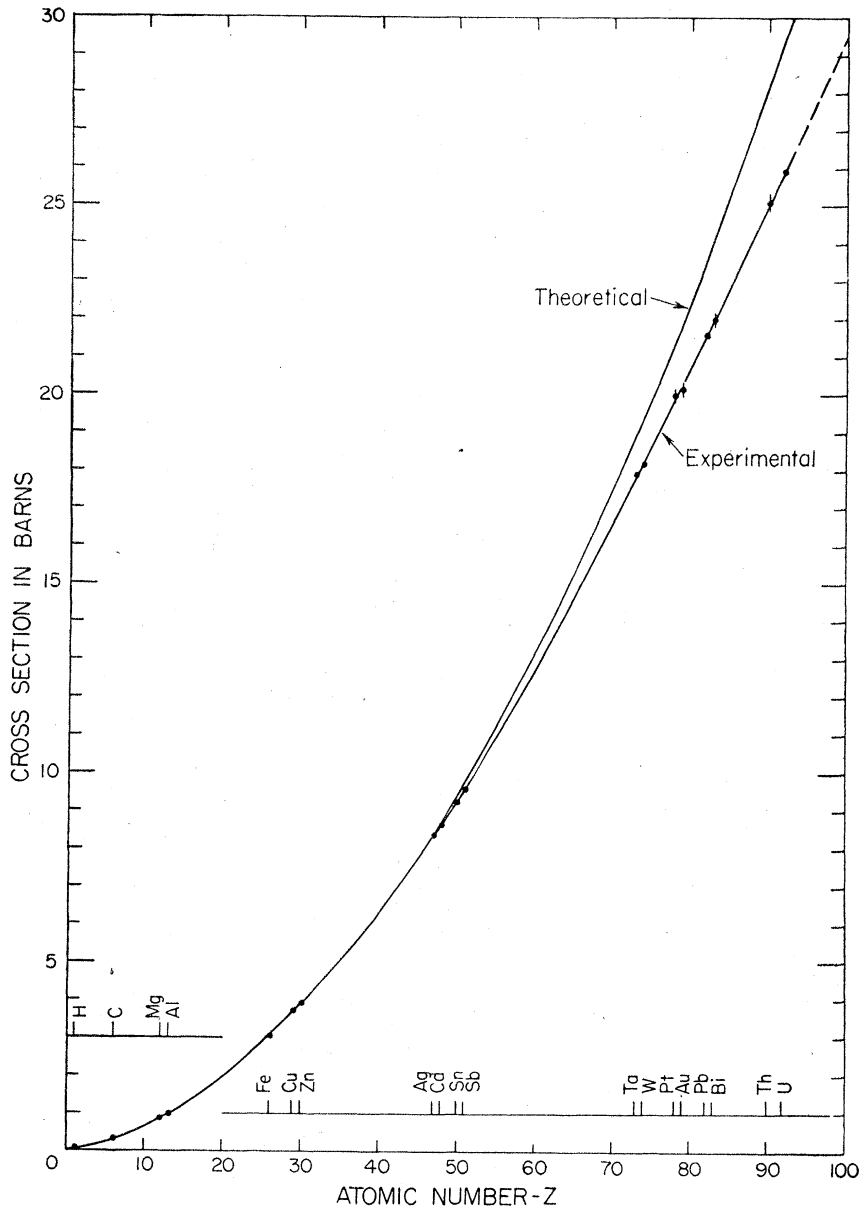


FIG. 4. Total cross sections for 19.5-Mev quanta *vs* *Z*. Those statistical errors which exceed the radii of the circles are indicated.

of residual nuclei, combined with theoretical conclusions.<sup>18</sup> For the heavier elements account is taken of both the rise in integrated cross section and slow decrease in the energy at which the cross section is maximum, as functions of *Z*.

Total experimental cross sections are given in Table II. The errors cited are obtained from internal consistency in the six or more runs made for each absorber. These exceed the statistical errors which would be obtained from the counts themselves by two or three times. The experimental cross section for hydrogen was calculated from the carbon and polyethylene

absorber data; this entailed a considerable statistical error despite the fact that additional sets of these runs were made. In Fig. 4 the experimental and theoretical total cross sections per atom *vs* *Z* are plotted.

### III. INTERPRETATION OF THE EXPERIMENTAL DATA

The sum of the Compton and pair cross sections was isolated by subtracting the known theoretical-empirical data of the competing reactions from the total. The relatively small magnitude of these competing cross sections permits a considerable tolerance in their values.

#### A. Compton Cross Section

For low *Z* elements the Bethe-Heitler formula was employed to remove the small pair cross section from

<sup>18</sup> J. Heidmann and H. A. Bethe, Phys. Rev. 84, 274 (1951); J. S. Levinger and H. A. Bethe, Phys. Rev. 85, 577 (1952).

the Compton-pair sum. This formula, although derived with the Born approximation, is very accurate near 20 Mev for light elements, as shown in the next section. (Actually the very slight correction of Eq. (8) was made before subtracting.) The cross section which remained was divided by  $Z$ , and the result is shown graphically in Fig. 5. Those systematic errors which occur from the assumption of a 50 percent uncertainty in the photonuclear cross sections were added linearly to the standard deviations; the weighted mean of the Compton cross section per electron was then found to be  $0.03025 \pm 0.00065$  barn. The Klein-Nishina total Compton cross section per electron, 0.03084 barn, lies within the error cited. Higher order radiative corrections, if applied to the theoretical formula, would not be expected to alter its value by more than about one percent at this energy.<sup>19</sup>

## B. Pair Production Cross Section

### 1. Failure of the Born Approximation

As is evident from Fig. 4 the difference between the theoretical and experimental total cross section is an increasing function of  $Z$ . This is attributed to only the pair cross section, since the theories of the other processes either are well established or their cross sections are relatively insignificant. It is, of course, assumed that the Klein-Nishina Compton cross section, verified in this experiment, retains its validity for high  $Z$  elements. However, like the Bethe-Heitler formula, planar wave functions are employed in the calculation. An error therefore occurs for strongly bound electrons; but this has such a negligible effect on the total Compton

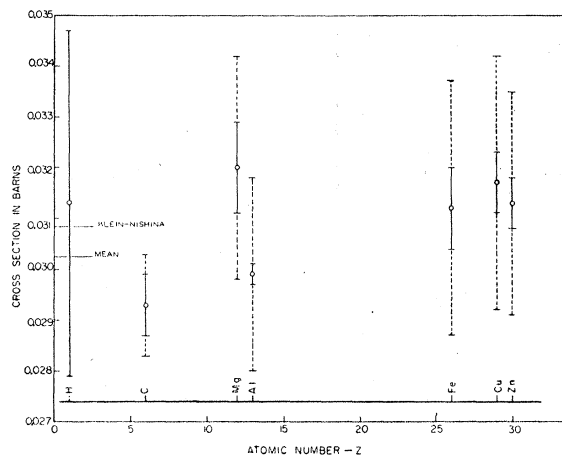


FIG. 5. Total experimental atomic cross sections, minus the sum of the photoelectric (Hall), pair (Bethe-Heitler), triplet (Wheeler-Lamb), and photonuclear (semi-empirical) cross sections, this difference divided by  $Z$ . Errors resulting from the assumption of a 50 percent uncertainty in the photonuclear cross sections are shown (dotted) added linearly to the standard deviations. The integrated Klein-Nishina cross section per electron is compared with the weighted mean.

<sup>19</sup> L. M. Brown and R. P. Feynman, Phys. Rev. 85, 231 (1952).

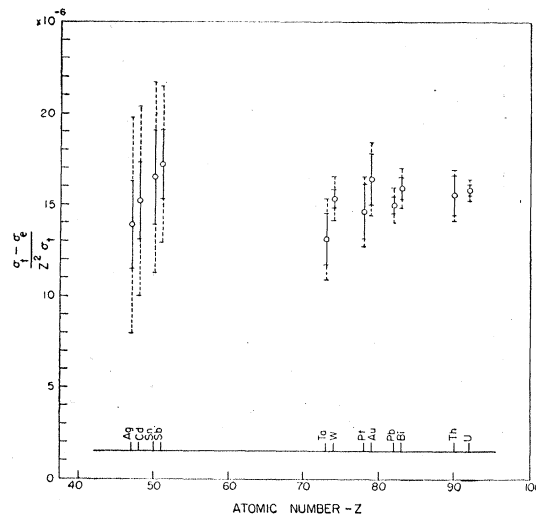


FIG. 6. Fractional difference between the theoretical (Bethe-Heitler) and experimental pair cross sections divided by  $Z^2$ . Errors resulting from the assumption of a 50 percent uncertainty in the photonuclear cross sections are shown (dotted) added linearly to the standard deviations.

cross section *per atom*, which in turn is overwhelmed by the relatively large pair cross section for high  $Z$  elements at 19.5 Mev, that it may be ignored completely.

A plot of the theoretical-experimental differences *vs*  $Z$  reveals a parabolic shape. In Fig. 6 these fractional differences, divided by  $Z^2$ , are plotted for those high  $Z$  elements which were measured.

The error in the Bethe-Heitler formula for the pair cross section may be stated, from these data, as

$$(\sigma_{\text{BH}} - \sigma_{\text{pair}}) / \sigma_{\text{BH}} = (1.55 \pm 0.1) \times 10^{-5} Z^2, \quad (8)$$

to a first approximation. This error is attributed to the failure of the Born approximation condition  $Z/137 \ll v/c$  (where  $v$  is the velocity of the particle) for each pair electron, even at the extreme relativistic recoil velocities expected for nearly all electrons produced by 19.5-Mev quanta.

The Born approximation failure cannot be shared by the triplet calculation, since the Coulomb field of an atomic electron would barely distort the wave function of pairs produced at this energy as does a high  $Z$  nuclear field.

### 2. Further Comparisons with Theory and Experiment

The sign of the correction of Eq. (8) agrees with the pair production equation of Maximon, Davies, and Bethe in which Coulomb wave functions were employed subject to the condition that the quantum energy,  $\epsilon \gg m_0 c^2$ .<sup>6</sup> Their correction also increases with  $Z^2$  to a first order, being somewhat less for heavy elements; furthermore, it is greater in magnitude, e.g., 20 percent for lead instead of 10.4 as found from Eq. (8). This discrepancy is due possibly to the failure of the energy condition in the theoretical calculation, as noted by

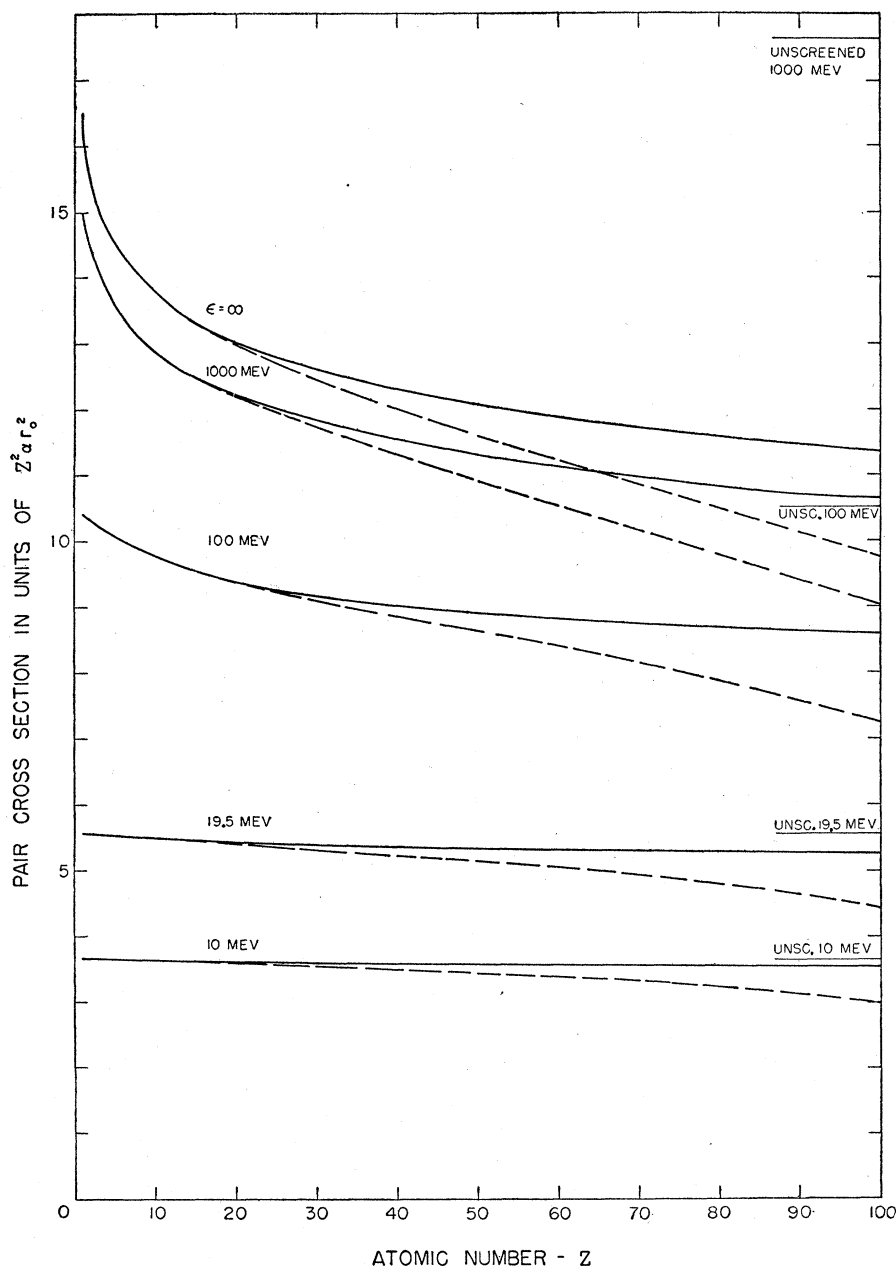


FIG. 7. Pair cross sections of all elements at several quantum energies ( $\alpha=1/137$ ). The solid curves are based on the Bethe-Heitler formula. The dotted curves are corrected values from

$$\sigma_{\text{pair}} = \sigma_{\text{BH}}(1 - 1.5 \times 10^{-5} Z^2),$$

which is assumed to be valid at all extreme relativistic energies.

the authors. An exact theory would have to consider the effect producing the *positive* deviations with respect to the Born approximation result, which were calculated by Hulme and Jaeger at low energies,<sup>20</sup> and in basic agreement with experiment.<sup>21</sup> The smaller magnitude of the Maximon-Davies-Bethe correction for lead at

<sup>20</sup> H. R. Hulme and J. C. Jaeger, Proc. Roy. Soc. (London) **153**, 443 (1936). J. C. Jaeger [Nature **137**, 781 (1936)] found a positive  $Z^2$  correction at 1.53 Mev. These calculations employed exact wave functions but still were subject to about 5 percent error; minor electronic transitions were neglected because of the extreme complexity of the computation.

<sup>21</sup> Hahn, Baldinger, and Huber, Helv. Phys. Acta **24**, 324 (1951); I. E. Dayton, Phys. Rev. **89**, 544 (1953).

88 Mev and 280 Mev (11.8 and 10.0 percent, respectively) is not at variance with the results of experiments performed at these energies.<sup>22</sup>

Considering the experimental data in several high energy regions,<sup>13,14,22</sup> including the pair track measurements of Emigh in the 50 to 300-Mev range,<sup>23</sup> it is probably reasonable to state the high energy discrepancy with the Born approximation theory as being on the order of  $1.5 \times 10^{-5} Z^2$ . In Fig. 7 the Bethe-

<sup>22</sup> J. Lawson, Phys. Rev. **75**, 433 (1949); DeWire, Ashkin, and Beach, Phys. Rev. **83**, 505 (1951).

<sup>23</sup> C. R. Emigh, Phys. Rev. **86**, 1028 (1952).

Heitler cross section is shown for all  $Z$  at several high energies, as adjusted by this assumed correction.

The author wishes to express his sincere thanks to Dr. G. H. Tenney and Mr. J. W. Dutli for their support and for making this project possible in the Radiographic Research Group of the Los Alamos Scientific Laboratory. The work of the Chemistry-Metallurgy Division in fabricating the absorbers at high purity and providing chemical analyses is appreciated.

APPENDIX. RATIO OF COUNTS DUE TO SECONDARY RADIATION TO THAT OF PRIMARY RADIATION:  $C_s/C_p$

The number of counts resulting from primary radiation falling on a point in the detector may be written

$$C_p = k_0 \int_{\epsilon_T}^{\epsilon_M} I_e \sigma_e d\epsilon, \quad (A1)$$

where  $I_e = k_1(\epsilon_M - \epsilon)^{\frac{1}{2}} e^{-\mu_L R_0}$  = bremsstrahlung energy distribution function near cutoff, partially attenuated by absorber;  $\sigma_e = k_2(\epsilon - \epsilon_T)^{\frac{3}{2}} = C^{12}(\gamma, n)$  cross section near threshold;  $\mu_L$  = linear absorption coefficient of absorber, assumed constant within the detecting band,  $\epsilon_M - \epsilon_T$ ;  $R_0$  = absorber thickness; and  $k_0, k_1, k_2$  = constants. Integrating, one obtains

$$C_p = k_0 k_1 k_2 \frac{\pi}{8} (\epsilon_M - \epsilon_T)^2 e^{-\mu_L R_0}. \quad (A1a)$$

The number of counts due to secondary radiation (see Fig. 8) is

$$C_s = k_0 \int_0^{R_0} \int_{\epsilon_T}^{\epsilon_M} \int_0^{\Omega_{\max}} I_{R\epsilon\Omega} \sigma_e d\Omega d\epsilon dR, \quad (A2)$$

where  $I_{R\epsilon\Omega} = k_1(\epsilon_M - \epsilon - P\theta^2)^{\frac{1}{2}} (n_{R\Omega} \sigma_\theta / R^2) e^{-\mu_L R_0}$  = energy distribution of scattered radiation (degraded bremsstrahlung);  $P = \epsilon_M^2 / 2m_0 c^2$ ;  $\sigma_\theta$  = Klein-Nishina scattering cross section ( $= r_0^2$  for small  $\theta$ ),  $R$  = distance between

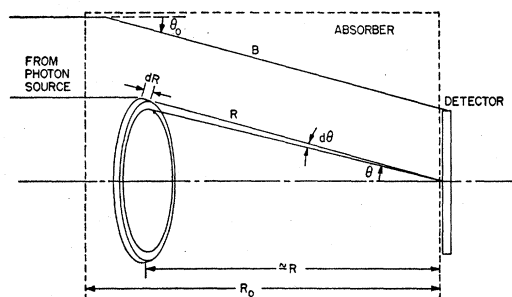


Fig. 8. Scattering from an infinitely distant source of photons into a detector which responds only to radiation of  $\epsilon > \epsilon_T$ , where  $(\epsilon_M - \epsilon_T) \ll \epsilon$ . The volume of scattering centers, which contribute to detected secondary radiation, is confined within a cone of revolution bounded by  $B$ .  $n_{R\Omega} d\theta dR$ , the number of scattering centers between  $\theta$  and  $\theta + d\theta$ , and  $R$  and  $R + dR$ , lies within the ring shown. The maximum angle of detected scattered radiation,  $\theta_0$ , is exaggerated in this diagram.

scattering point and detector point. The small-angle form of the Compton energy shift for high energy quanta is  $P\theta^2$ . It occurs in the scattered bremsstrahlung distribution, since each quantum which emerges at an angle  $\theta$  suffered an energy loss of  $P\theta^2$  in the scattering process. The factor  $e^{-\mu_L R_0}$  represents the net attenuation in the absorber of both the detected scattered radiation and the primary radiation which produced it.  $n_{R\Omega} d\Omega dR$  is integrated over  $\varphi$  to yield  $n_{R\theta} d\theta dR = 2\pi n_e R^2 \theta d\theta dR$ , where  $n_e$  = density of scattering centers (electrons/cm<sup>3</sup>).

The integrations over  $\theta$ ,  $\epsilon$ , and  $R$  are performed, keeping in mind that the upper limit of the  $\theta$ -integral is  $[(\epsilon_M - \epsilon)/P]^{\frac{1}{2}}$ ; i.e., a singly scattered quantum of energy  $\epsilon$  could never have been the result of a deflection greater than this angle. The integration yields

$$C_s = \frac{\pi^2}{24} k_0 k_1 k_2 n_e r_0^2 \frac{(\epsilon_M - \epsilon_T)^3}{P} R_0 e^{-\mu_L R_0}. \quad (A2a)$$

Writing  $P$  in terms of  $\theta_0$ , the maximum scattering angle, as  $(\epsilon_M - \epsilon_T)/\theta_0^2$ , there follows

$$C_s/C_p = \frac{1}{3} \pi n_e r_0^2 R_0 \theta_0^2. \quad (A3)$$